

# Quasiphase transition of a single-file water chain influenced by atomic charges in water model using orientational-biased replica exchange Monte Carlo simulations

Liang Zhao<sup>a, †</sup>, Junqing Ni<sup>a</sup>, Zhi Zhu<sup>b</sup>, Yusong Tu<sup>a</sup> and Chunlei Wang<sup>c, †</sup>

<sup>a</sup>College of Physical Science and Technology & Microelectronics Industry Research Institute, Yangzhou University, Jiangsu, 225009, China

<sup>b</sup>School of Optical-Electrical Computer Engineering, University of Shanghai for Science and Technology, Shanghai, 200093, China

<sup>c</sup>College of Sciences, Shanghai University, Shanghai, 200444, China

†Corresponding authors: zhaoliang@yzu.edu.cn, wangchunlei1982@shu.edu.cn

## Abstract

The recently observed temperature-dependent quasiphase transition of the single-file water chain confined within a carbon nanotube in experiments has been validated by simple lattice theory and molecular dynamic simulations. It has been pointed out that the atomic charge in water models is an important issue, yet how the value will affect the structural details and thermodynamic properties of quasiphase transitions has not been fully revealed. In this work, we performed orientational-biased replica exchange Monte Carlo simulations in the canonical ensemble to explore the quasiphase transition of a single-file water chain affected by the atomic charges in SPC/E water model. Using the value of atomic charge reported from literature, we reproduce three distinct quasiphases comprising a fully hydrogen-bonded water chain at lower temperatures, a more ordered dipolar orientation along the  $x$ -axis at intermediate temperatures, and a completely disordered structure at higher temperatures. Then by increasing the atomic charge value, we find that the fragmentation of the entire water chain into shorter water segments, the orientational ordering of water dipoles, and the transition towards complete disorder are all inhibited. Consequently, the transition temperatures between three quasiphases have been shifted to higher temperatures. The thermodynamic analysis demonstrates that the larger atomic charge enhances the hydrogen bonding between neighbouring water molecules also the electrostatic attraction within the water chain, extending the spatial correlation of a pair of water dipoles. These findings shed light on the vital role of atomic charges of water models and electrostatic interaction in regulating the behavior of single-file water chain under nanoconfinement.

## I. INTRODUCTION

Understanding the behavior of water confined within nanoscale environments [1-4], particularly in carbon nanotubes (CNTs) [5-8], provides valuable insights into the exploration of extraordinary transport properties [9-15] of nanopores or biological channels, as well as the manufacture of promising water-mediated applications such as signal conversion [16] and desalination devices [17]. Water molecules confined in CNT exhibit distinct structures and dynamic behaviors compared to those in bulk [7, 18]. When the CNT diameter decreases to less than 1 nm, the mutual passage of molecules is prohibited, and a single-file water chain is formed. The neighbouring water molecules are tightly connected by hydrogen bonds (HBs), and their dipoles are approximately aligned along the tube axis. Among various theoretical and computational investigations, the one-dimensional water chain model, despite its simplicity, offers insights into the interaction between water molecules and how these interactions

influence the overall behavior of the water chain. Koflinger *et al.* introduced a one-dimensional (1D) dipole lattice model, in which each molecule is represented as a point dipole positioned at a regular lattice site [19-22]. The water chain can thus be viewed as several ordered segments consisting of equally oriented dipoles along the axis, separated by defects with vertical dipole orientations. The total energy is expressed as the sum of internal energies of segments and their dipole-dipole type interactions. This model has been successful in reproducing the filling-empty transition, bistability of particle number distribution, and static dielectric response to an external field. A more realistic water chain model developed by Sahoo [23] and Serwatka *et al.* [24], treats water molecules as identical asymmetric rigid tops with fixed equal interdistances and orientational freedom in space, interacting through two-body or many-body water potentials [24]. Based on this model, quantum mechanical descriptions of the water chain, including HB ordering at shorter interdistances and dipolar ordering at larger distances, have been well reflected in the study of ground state behavior using the path integral ground state approach [23] or the density matrix renormalization group method [25]. When a more detailed description of the structure or dynamics of a single-file water chain is needed, such as the water gating and flipping [26-28], proton transfer process [9, 10, 29], the interaction sites of oxygen and hydrogen atoms should be explicitly considered and various water models have been employed in computational simulations.

Recently, a temperature-dependent quasiphase transition of the single-file water chain was first reported inside the (6, 5)-SWCNT by Ma *et al.* [30]. They realized the direct comparison of photoluminescence spectra of empty and water-filled SWCNTs, and observed an additional stepwise spectrum shift for water-filled SWCNT at  $\sim 150$  K. Using molecular dynamics (MD) simulations, they attributed the quasiphase transition to the temperature-dependent changes in orientational ordering of water dipoles. Druchok *et al.* further discussed in detail the existence of quasiphase transition by MD simulations of water molecules encapsulated inside (6, 5)-SWCNT [31]. They not only reproduced the quasiphase transition given by Ma *et al.*, most importantly, proposed a simple lattice model based on statistical mechanics. In this model, coplanar water dipoles were rendered on lattice sites of a straight line, with each site assigned three states subjected to configurational restrictions. The partition function of the water chain was obtained by adding the contributions from short-range nearest neighbour interaction and long-range dipole-dipole interaction as well as the rotational entropy contributions. The quasiphase transition and the simple lattice model has been generalized to another polar molecule, ammonia, expanding the category of quasiphase transition [32]. In these works, the atomic charge in water models is considered to be an important issue and the values have been revised according to quantum chemistry calculations. The calculated values are found to be significantly smaller than default values [30, 31], due to the coupling between the molecular orbitals of SWCNT and water molecules [33]. For example, the atomic charge of oxygen atom  $q_O$  in extended simple point charge (SPC/E) water model is revised to  $-0.4348e$ , less than the default value of  $-0.8476e$  [31]. However, the impact of atomic charges in water models on the quasiphase transition behavior of a single-file water chain, such as the structural details and thermodynamic properties, has not been fully revealed.

To address this issue, we perform the orientational-biased replica exchange Monte Carlo (MC) simulation of a single-file water chain of SPC/E water model with varied values of atomic charges. Using the atomic charge values as reported in literature, we first reproduce the quasiphase transition including a fully hydrogen-bonded water chain at lower temperatures, a

more ordered dipolar orientation along the  $x$ -axis at intermediate temperatures, and a completely disordered structure at higher temperatures. Then, by increasing the atomic charge, we find that the fragmentation of the entire water chain into shorter water segments, the orientational ordering of water dipoles, and the transition towards complete disorder are all inhibited. Consequently, the transition temperatures between three quasiphases have been shifted to higher temperatures. It is demonstrated that the larger atomic charge enhances the hydrogen bonding between neighbouring water molecules also the electrostatic attraction within the water chain, therefore extending the spatial correlation of a pair of water dipoles. These findings emphasize the importance of atomic charges of water models in and electrostatic interaction in regulating the behavior of single-file water chain under nanoconfinement.

## II. MODEL AND METHODS

The chain of  $N = 40$  water molecules is arranged along the one-dimension  $x$ -axis within a finite length  $L = 24$  nm without periodic boundary condition, as shown in Fig. 1. Two hard spheres are fixed at the two endpoints to confine water molecules within the interval. The movement of each water molecule is restricted along the  $x$ -axis for simplicity while the spatial orientation is free. Initially, water molecules are positioned and oriented randomly. The geometry of water molecule is modeled by the rigid SPC/E model, where the H-O-H bond angle is  $109^\circ 47'$  and the O-H bond length is 0.1 nm. The Lennard-Jones (LJ) parameters for oxygen are  $\epsilon_{OO} = 0.636$  KJ/mol and  $\sigma_{OO} = 0.315$  nm, and oxygen-oxygen LJ interaction is described by  $E_{LJ} = 4\epsilon_{oo} \left[ \left( \frac{\sigma_{oo}}{r} \right)^{12} - \left( \frac{\sigma_{oo}}{r} \right)^6 \right]$ . The LJ parameters of hydrogen are neglected. The electrostatic interaction between two charges is given by  $E_{ele} = \frac{1}{4\pi\epsilon_0} \frac{q_i q_j}{r_{ij}}$ , where  $i, j$  denote the O or H atoms and the electrostatic charge  $q_O = -Q$ ,  $q_H = +0.5Q$ . No cutoff radii are used in the calculations of LJ and electrostatic interactions. The value of  $Q$  is varied from  $0.2e$  to  $0.8e$  with the increasement of  $0.1e$ , which covers a large range of charges obtained from different quantum calculations. The  $Q = 0.4328e$  given by Druchok *et al.* [31] is taken as a reference system.

The hydrogen bond (HB) is defined in terms of a geometric criterion: the O...O distance of a pair of water molecules is less than a cutoff distance  $R_c$  and O-H...O angle is less than  $30^\circ$ . The  $R_c$  is determined as the first minimum in the radial distribution function. There is a slight decrease of  $R_c$  with the increase of  $Q$ , and we set  $R_c = 0.40$  nm for  $Q = 0.2e, 0.3e$  and  $0.4e$ ,  $R_c = 0.35$  nm for  $Q = 0.4328e, 0.5e, 0.6e, 0.7e$  and  $0.8e$  for accuracy (see radius distribution functions in PS. 1 of the Appendix). The HB energy of a pair of hydrogen-bonded water molecules is defined as the sum of LJ and electrostatic energies.

In the canonical ensemble (NVT) Monte Carlo simulations, three types of sampling algorithms are employed including traditional Metropolis-based translation and rotation, orientational-bias (OB) and replica exchange (RE) methods. OB is used to sample the configurations with HBs, which strongly depends on the relative molecular orientation [34]. RE shows the advantage in overcoming systems with possible multiple barriers [35] and outputting configurations at different temperatures in a single task submission. We have found that the combination of these algorithms is able to search the stable system states with lower energy and produce a more continuous sampling of potential energy, heat capacity and orientational ordering of the water chain (see comparisons of Metropolis sampling, Metropolis + OB and Metropolis + OB + RE

for the reference system of  $Q = 0.4328e$  in PS. 2 of the Appendix).

A single MC sweep consists of three types of MC moves: (i) Metropolis translational and orientational moves, (ii) Metropolis translational and orientational moves with the OB method, and (iii) RE swap. Trial moves (i) and (ii) are performed randomly within  $2N = 80$  steps, followed by using one RE swap (iii). For the translational move, it is restricted along the  $x$ -axis and initial maximum allowed displacement of the oxygen atom is 0.015 nm. For the orientational move, one of three Cartesian axes is randomly chosen and initial maximum rotation angle is  $5^\circ$ . These two parameters are automatically adjusted to give the acceptance ratio of about 30%. For the OB method, 5 trial orientations are selected to construct the Rosenbluth factor. For the RE method,  $M = 140$  replicas are used ranging from temperature  $T = 1$  K to 279 K with the equal spacing of 2 K. Each replica exchanges the configuration with its two neighbours, that is,  $M$  replicas can be paired up in two ways: [(1, 2), (3, 4), ...] or [(2, 3), (4, 5), ...] where the configurations of two replicas in the same parenthesis will be exchanged and the two ways are randomly chosen [36]. The total MC sweeps are  $5 \times 10^6$  and the configurations in the last  $1 \times 10^6$  sweeps are collected per 100 sweeps for analyses.

### III. RESULTS AND DISCUSSION

#### A. Characterization of a single-file water chain

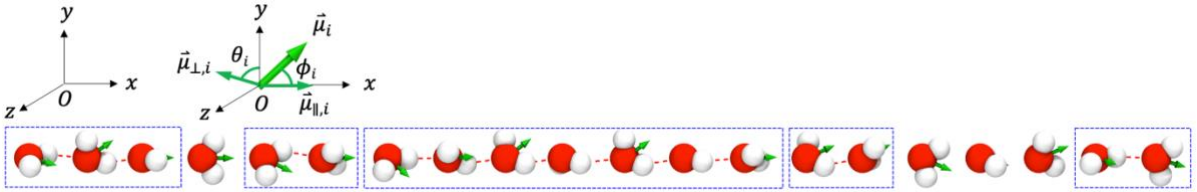


**FIG. 1.** Illustration of the configuration of a single-file water chain. Only twenty water molecules are shown here for convenience of display. The green vector  $\vec{\mu}_i$  represents the dipole of a water molecule indexed by  $i$ , with the tangent component  $\vec{\mu}_{\parallel,i}$  (projection of  $\vec{\mu}_i$  to the  $x$ -axis) and normal component  $\vec{\mu}_{\perp,i}$  (projection of  $\vec{\mu}_i$  into the  $yOz$  plane). Two polar angles  $\phi_i$  and  $\theta_i$  denote the angle between  $\vec{\mu}_i$  and  $+x$  direction, and that between  $\vec{\mu}_{\perp,i}$  and  $+y$  direction, respectively. The red dashed line connecting a hydrogen atom (white sphere) and an oxygen atom (red sphere) denotes the HB. The water molecules within a blue dashed frame represent a water segment, where neighbouring water molecules are connected by the HB.

In order to characterize the configuration of a single-file water chain, the following quantities are introduced: (I) A water segment is defined as a wire of water molecules where adjacent molecules are connected by HBs. According to this definition, water molecules are categorized into two groups: those within water segments and those not belonging to any water segment. Taking the configuration in Fig. 1 as an example, the whole water chain is divided into 5 water segments containing 16 water molecules in total and 4 individual water molecules out of any segments. The longest water segment is 7 water molecules' long; (II) The orientation of a water molecule indexed by  $i$  is described by two polar angles, with  $\phi_i$  denoting the angle between the dipole  $\vec{\mu}_i$  and  $+x$  direction and  $\theta_i$  denoting the angle between  $\vec{\mu}_{\perp,i}$  and  $+y$  direction. The average dipole angle of water chain is given by  $\bar{\phi} = \sum_{i=1}^N \phi_i / N$ ; (III) The normal component of dipole vector of individual water molecules is  $\mu_{norm} = |\mu_{\perp}| / \mu$ , and the tangent component of the total dipole vector of the water chain is  $\mu_{tang} = \overline{\mu_{\parallel}^{total}} / (N\mu)$ , where the overline

represents the mean value. These two definitions are same to those used in Ma's and Druchok's work; (IV) The average available space of a water molecule in water segments is defined by the average oxygen-oxygen distance of a HB, and that of a water molecule out of water segments is estimated by the half of the sum of oxygen-oxygen distances with its two neighbouring molecules.

## B. The quasiphase transition for $Q = 0.4328e$

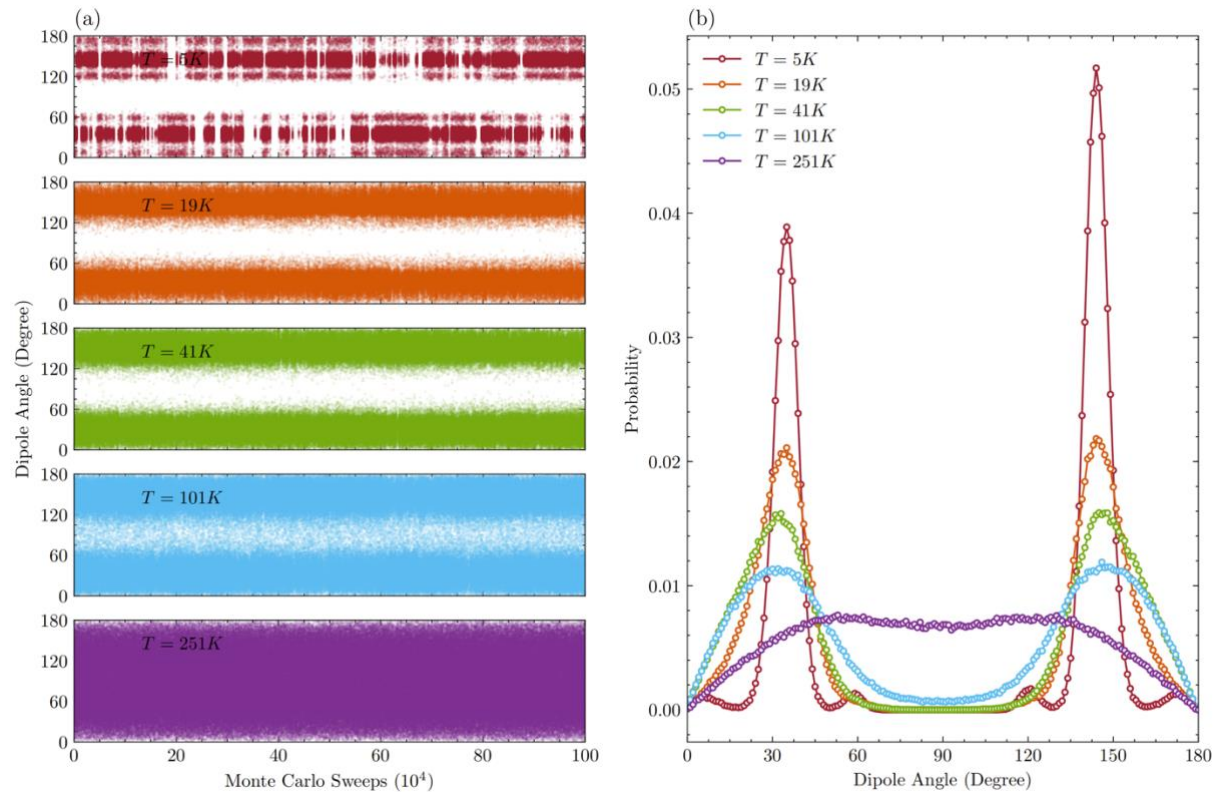


**FIG. 2.** (a) Scatter plots and (b) probability distributions of dipole angles of the water chain with respect to  $+x$  direction at five typical temperatures  $T = 5$  K, 19 K, 41 K, 101 K and 251 K.

It has been proved that the SPC/E water model with a revised  $Q = 0.4328e$  shows the quasiphase transition in nanochannels, despite that this value is smaller than the default value of  $0.8476e$ . Therefore, we first check the phase behavior of the single-file water chain using  $Q = 0.4328e$ . Figure 2 shows the scatter plots and probability distributions of the water dipole angle  $\phi_i$  at five typical temperatures. At a lower temperature  $T = 5$  K, the dipole angles mainly fall within two intervals of  $(0^\circ, 60^\circ)$  and  $(120^\circ, 180^\circ)$ , representing water dipoles oriented closely along the  $+x$  direction and its opposite direction. These symmetrical orientations are commonly achieved through water flipping. As the temperature increases, the boundary between these two intervals gradually diffuses and vanishes at a higher temperature  $T = 251$  K, indicating the increased orientational freedom for water molecules. These changes become evident in the probability distribution of dipole angles shown in Fig. 2(b). Two sharp peaks are observed around  $37^\circ$  and  $142^\circ$  at  $T = 5$  K. When  $T$  increases, the peak positions remain unchanged while their widths broaden, resulting in a larger fluctuation in dipole orientation around both  $37^\circ$  and  $142^\circ$ . From  $\sim 101$  K, the dipole orientation within the interval of  $(60^\circ, 120^\circ)$  emerges, and the dipole angle exhibits a relatively flat distribution at 251 K. This indicates that the ordered

arrangement of water chain gradually diminishes from 101 K, an indication of the order-disorder transition.

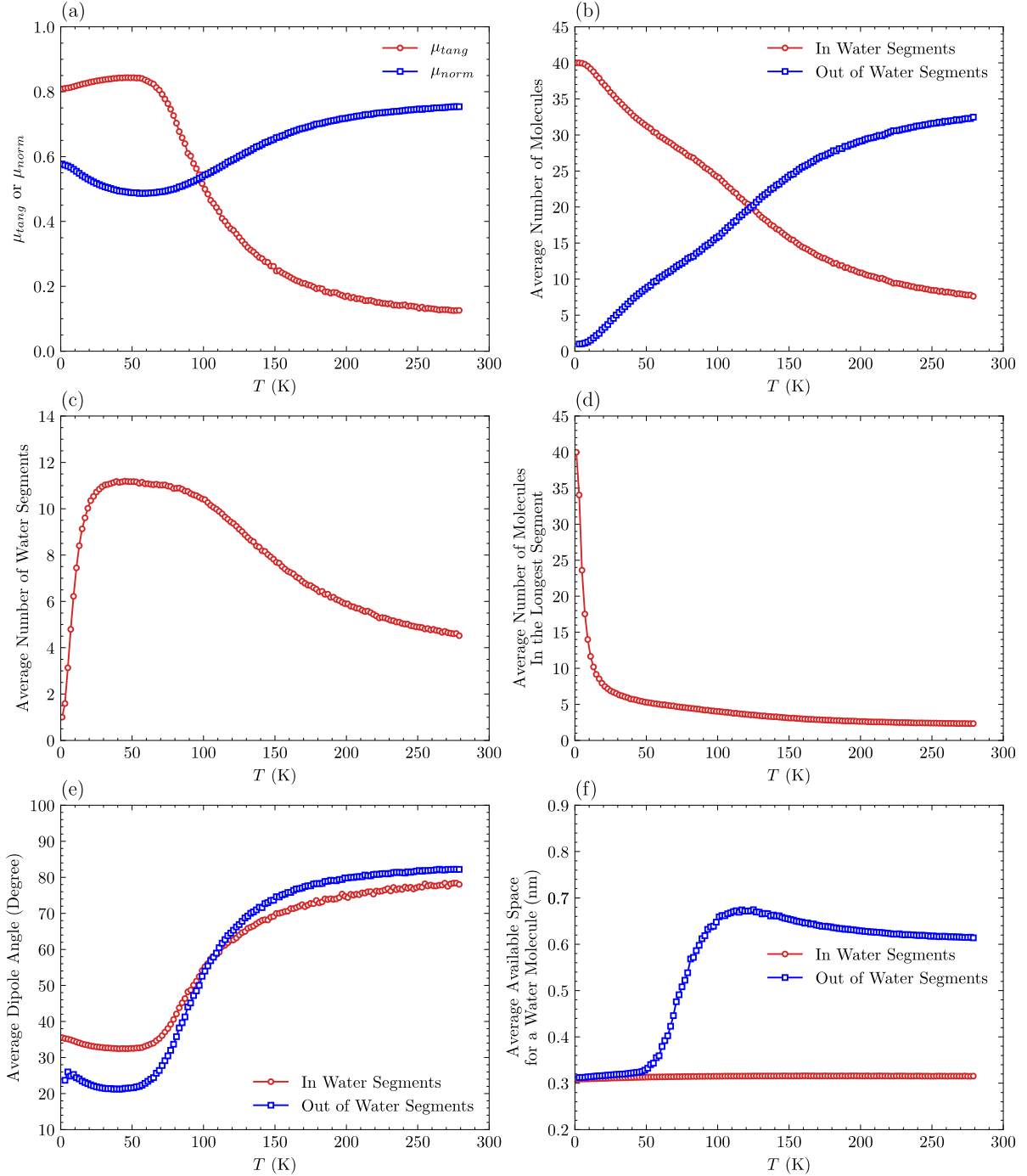


**FIG. 3.** (a) The average value of the normal component of individual water molecules  $\mu_{norm}$  and the average value of tangent component of the total dipole of the water chain  $\mu_{tang}$ . Configurational details of the water chain with respect to temperature, including (b) average number of water molecules in and out of water segments, (c) average number of water segments, (d) average number of water molecules within the longest water segment, (e) average dipole angle of water molecules within and out of water segments, and (f) average available space for a water molecule in and out of water segments. These average values are averaged over water chain configurations under the condition  $\bar{\phi} < 90^\circ$  and the errors are shown by the shaded areas.

We first show the ordering of the whole water chain by calculating the  $\mu_{tang}$  and  $\mu_{norm}$ . As discussed above, the water chain prefers two symmetric orientations, we focus on the orientation along the  $+x$  direction for convenience. The configuration is considered if the average dipole angle  $\bar{\phi}$  is less than  $90^\circ$ . As shown in Fig. 3(a),  $\mu_{tang}$  decreases from  $T = 1$  K and reaches the maximum at  $T \sim 50$  K, accompanied by an increase of  $\mu_{norm}$  to the minimum. As  $T$  continues increasing, the  $\mu_{tang}$  experiences a rapid decay around 100 K. The trends observed in  $\mu_{tang}$  and  $\mu_{norm}$  are consistent with those given by Ma *et al.* (TIP3P water model with the revised charge) and Druchok *et al.* (SPC/E water model with the revised charge) via MD simulations.

Through a detailed analysis of the temperature-dependent water arrangement including dipole angle and water segment configuration, three distinct quasiphases denoted by I, II and III have been identified. In the quasiphase (I) at lower temperatures of several Kelvin, all water molecules are coordinated by HBs ( $T = 1$  K, see Fig. 3(b)), forming a whole water segment (Fig. 3(c)). As the temperature increases closely to 10 K,  $N \sim 39$  water molecules remain bonded by HBs (Fig. 3(b)). However, the whole water chain has been fragmented into 6 water segments (Fig. 3(c)), with the longest one containing an average of 14 water molecules (Fig. 3(d)). We note that the interdistance between water molecules is approximately 0.31 nm (Fig. 3(f)), which is less than the cutoff value for a HB. This means that the formation of multiple water segments is influenced by the reorientation of water molecules due to the increase of temperature. Indeed, the average dipole angle within water segments shows a slight decrease from  $35.5^\circ$  at 1 K to  $34.3^\circ$  at 11 K, and the dipole angle out of water segments also decreases to about  $24.4^\circ$  (Fig. 3(e)). This variation of water dipoles is consistent with the increase of  $\mu_{tang}$  also the decrease of  $\mu_{norm}$  in Figs. 3(a) and 3(b), indicating that water molecules are more oriented along the  $+x$  direction. In the intermediate quasiphase (II) at around 50 K, the number of water molecules outside water segments increases to 9, and the number of water segments rises to 11, with a decrease in the number of water molecules in the longest segment to 5. This indicates that more water molecules escape from the coordination of HBs, leading to the formation of multiple shorter water segments. The whole water chain shows a more ordered structure in orientation, evidenced by the minima of  $32.5^\circ$  and  $21.6^\circ$  in Fig. 3(e) and also the extrema in  $\mu_{tang}$  and  $\mu_{norm}$  in Fig. 3(a). The interdistance between water molecules remains below the HB cutoff value. Upon the rise of temperature toward 100 K, we can see a notable increase of available space for water molecules out of water segment, from 0.33 nm to about 0.7 nm (Fig. 3(f)), accompanied by a dramatic increase of water dipole angle to about  $60^\circ$  (Fig. 3(e)). In the quasiphase (III) at higher temperatures above 100 K, nearly half of water molecules are out of water segments (Fig. 3(b)), with the number of water molecules in the longest segment decreasing to 2 (Fig. 3(d)). More water molecules are free of HBs and the disordered structure is formed. The significant loss of hydrogen bonds dominates the quasiphase transition. When  $T$  reaches room temperature, water dipoles out of water segments tend to be oriented vertically to the  $+x$  direction than those in water segments, with their values of  $82^\circ$  and  $78^\circ$ , respectively.

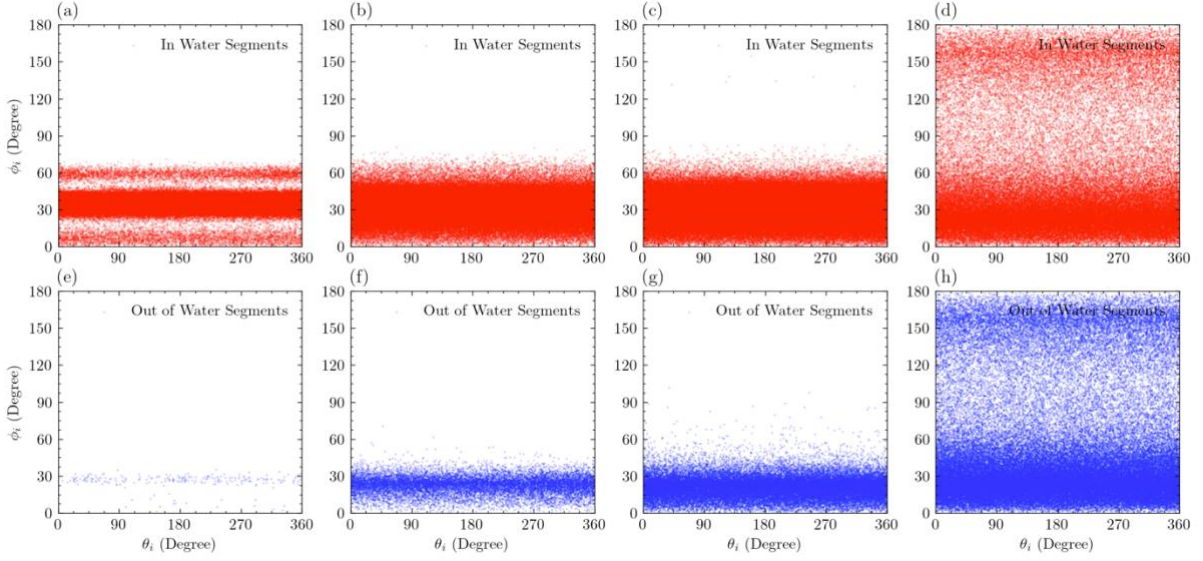


**FIG. 4.** Orientational maps of two polar angles,  $\theta_i$  and  $\phi_i$ , for water molecules at (a, e)  $T = 5$  K, (b, f) 19 K (c, g) 41 K and (d, h) 101 K. Upper panel: in water segments; Bottom panel: out of water segments. The two angles are defined in Fig. 1.

Figure 4 presents the orientational maps of two polar angles,  $\theta_i$  and  $\phi_i$ , for water molecules in and out of water segments at temperatures  $T = 5$  K, 19 K, 41 K and 101 K, encompassing quasiphases I, II and III. At all temperatures, the polar angle  $\theta_i$  shows a uniform distribution from  $0^\circ$  to  $360^\circ$ , indicating the absence of preferential directions for projected water dipoles in the  $y$ - $z$  plane normal to the  $+x$  direction. At  $T = 10$  K, most of water molecules are hydrogen-bonded, resulting in a higher density of dots scattered in Fig. 4(a) than in Fig. 4(d). The distribution of  $\phi_i$  for water dipoles in and out of water segments at  $T = 10$  K mainly fall within the ranges of  $(0^\circ, 60^\circ)$  and around  $30^\circ$ , respectively. As temperature increases, such as at  $T = 41$  K,  $\phi_i$  of a few water molecules exceeds  $90^\circ$ , an indication of water flipping. At a higher temperature of  $T = 101^\circ$ , a considerable number of water dipoles flip toward the  $-x$  direction, leading to a diffuse distribution of  $\phi_i$  (Figs. 4(d) and 4(h)). The temperature-dependent diffusion of  $\phi_i$  is consistent with the relatively large fluctuations of average dipole angle of water molecules in or out of water segments from about 50 K shown in Fig. 3(e).

With the description of structure and transition of quasiphases of the single-file water chain, now we turn to the temperature-dependent thermodynamic quantities and correlations. As shown in Fig. 5(a), the total potential energy shows an increase from about -250 KJ/mol to -50 KJ/mol across the temperature range primarily driven by electrostatic interactions, while the van der Waals interaction shows a weak repulsion with negligible positive values. Similarly, the HB energy between water pairs, increasing from -5.2 KJ/mol to -3.4 KJ/mol, is predominantly influenced by electrostatic attraction (Fig. 5(b)). We further calculate the heat capacity by the expression  $C_V = C_V^k + C_V^p = \frac{1}{2}RfN + \frac{\langle E_p \rangle^2 - \langle E_p^2 \rangle}{RT^2}$  [37], where the first term with freedom  $f = 4$  corresponds to the contribution from kinetic energy related to one translational freedom along the  $x$ -axis and three spatial rotational freedoms, and the second term is from the fluctuation of total potential energy. Fig. 3(c) shows two peaks at  $T \sim 10$  K and 100 K, dividing the temperature range into three regimes corresponding to three quasiphases. The presence of first peak at lower temperatures is noteworthy, as the heat capacity usually a constant (in the

ideal gas model) or increases with temperature (in the Einstein or Debye solid model). According to the structural analysis in Figs. 3 and 4, the whole HB bonded water chain breaks into a few water segments at  $T \sim 10$  K and forms a more ordered orientation along the  $+x$  axis meantime keeping the interdistance between water molecules unchanged. We therefore assume that the peak is Schottky-like heat capacity which is likely due to the excitation of rotational freedom in a few water molecules. The second peak is at  $T \sim 100$  K signifies the formation of disordered structure, as indicated in Fig. 3. In fact, the relative entropy  $\Delta S$  with reference to  $T = 1$  K, calculated by  $\Delta S(T) = \int_1^T \frac{C_V}{T} dT$ , continuously increases across the whole temperature range (Fig. 5(d)). This suggests that the structure of the single-file water chain continuously evolves toward disorder despite the existence of an ordered dipolar orientation of water molecules in quasihase II.

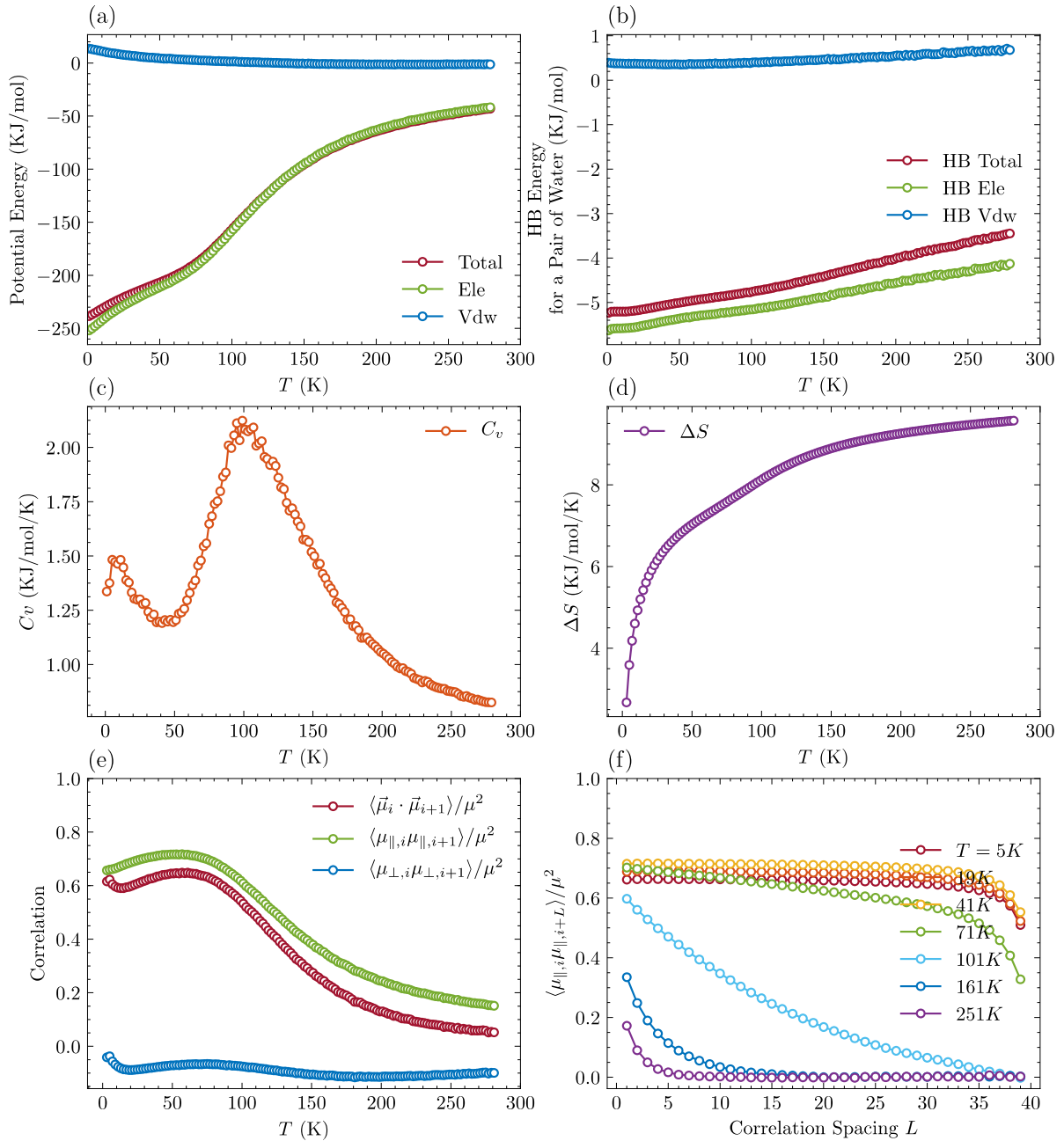


**FIG. 5.** Temperature dependent thermodynamic quantities and correlations. (a) Average total

potential energy ( $E_p$ ) of water chain decomposed into contributions from electrostatic ( $E_{ele}$ ) and van der Waals energies ( $E_{vdw}$ ) under  $E_p = E_{ele} + E_{vdw}$ . (b) Average HB energy between a pair of water molecules decomposed into contributions from electrostatic and van der Waals energies. (c) Specific heat capacity ( $C_v$ ) and (d) an estimated entropy ( $\Delta S$ ) relative to the entropy at  $T = 1$  K of the single-file water chain. (e) Correlations between neighbouring water molecules, including the correlations of dipole vector  $\vec{\mu}_i$ , tangent component  $\mu_{\parallel,i}$  and normal component  $\mu_{\perp,i}$ . (f) Temperature dependence of correlation of  $\mu_{\parallel,i}$  on two water molecules with the spacing  $L$  denoting the difference between indices of two molecules.

Figure 5(e) shows the correlations between dipoles of two water molecules. The positive and negative values of  $\mu_{\parallel,i}$  and  $\mu_{\perp,i}$  correlations indicate the staggered arrangement of neighbouring water dipoles. For  $T < 10$  K, the decrease of  $\mu_{\perp}$  correlation dominates the  $\vec{\mu}$  correlation despite that there is an increase in  $\mu_{\parallel}$  correlation. This confirms that neighbouring water dipoles are more aligned along the  $x$ -axis, as shown in Fig. 3(e). Meantime, there is an increased relative rotation on  $x$ -axis, making a more negative value of  $\mu_{\perp}$  correlation (see the relative angle of  $\mu_{\perp}$  of two neighbouring water dipoles in PS. 3 of the Appendix). When  $T$  is in the vicinity of 50 K, the water chain reaches the most ordered dipolar orientation, as evidenced by a peak in both  $\mu_{\parallel}$  correlation and  $\vec{\mu}$  correlation. For  $T \sim 100$  K, we can see the rapid decrease in  $\mu_{\parallel}$  and  $\vec{\mu}$  correlations, indicating the loss of HBs and a more disordered structure. The correlation of  $\mu_{\parallel}$  between neighbouring water molecules predominantly influences the water chain across the whole temperature range. As shown in Fig. 5(f), the  $\mu_{\parallel}$  correlation can nearly extend over the whole water chain at temperatures of 5 K, 19 K, 41 K, 71 K. A substantial decrease can be found at  $T = 101$  K, and when  $T = 251$  K the correlation spacing is reduced to about only 5 water molecules.

### C. The quasiphase transition for different values of $Q$

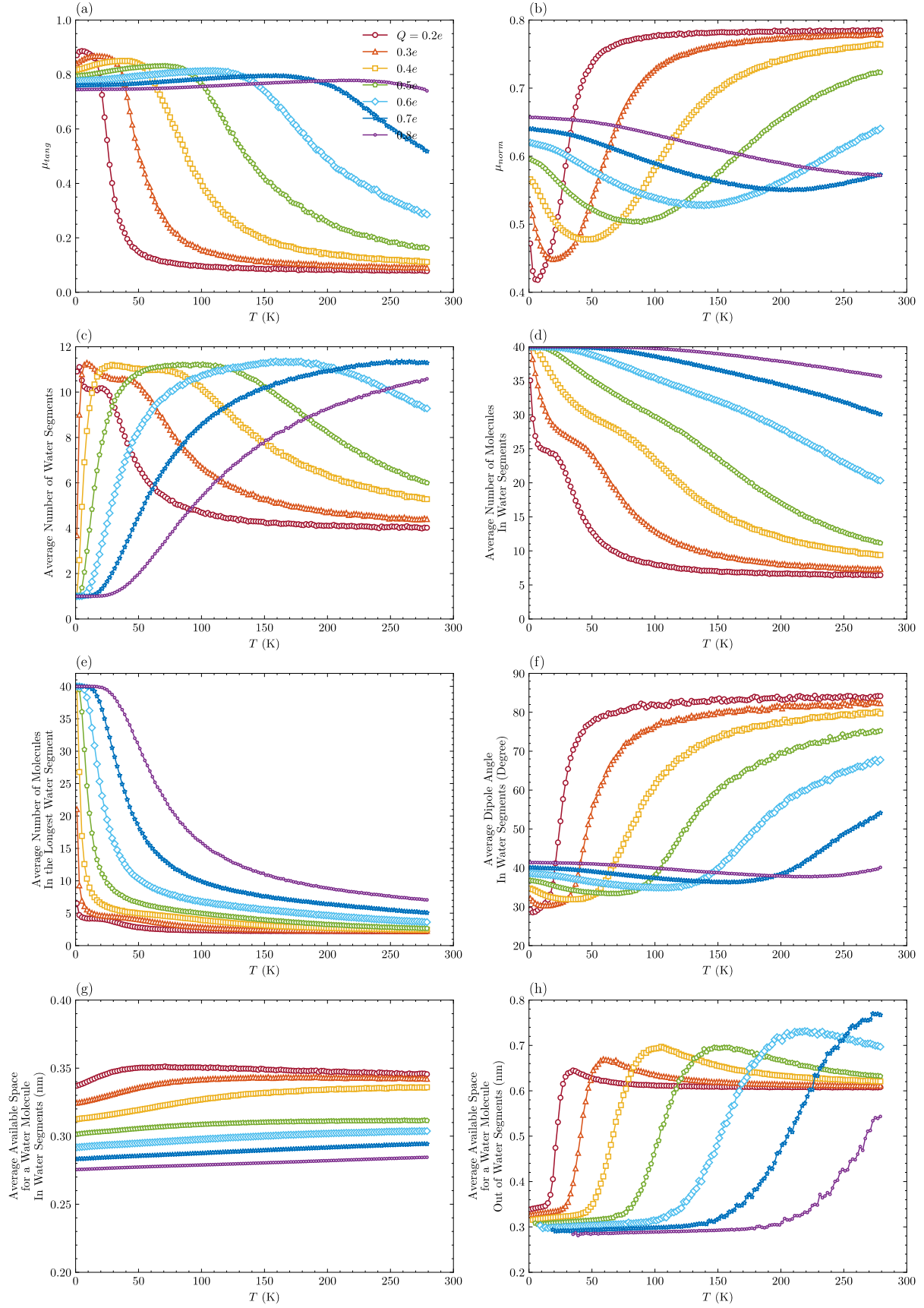


**FIG. 6.** Structural changes of the single-file water chain with respect to temperature, for  $Q$  ranging from  $0.2e$  to  $0.8e$  with the increasement of  $0.1e$ . (a)  $\mu_{tang}$ , (b)  $\mu_{norm}$ , (c) average number of water segments, (d) average number of water molecules in water segments, (e)

average number of water molecules in the longest water segment, (f) average dipole angle in water segments, average available space for a water molecule (g) in water segments and (h) out of water segments. In (h), a few dots at lower temperatures are missing as all the water molecules are coordinated by HB and no water molecules are out of water segments.

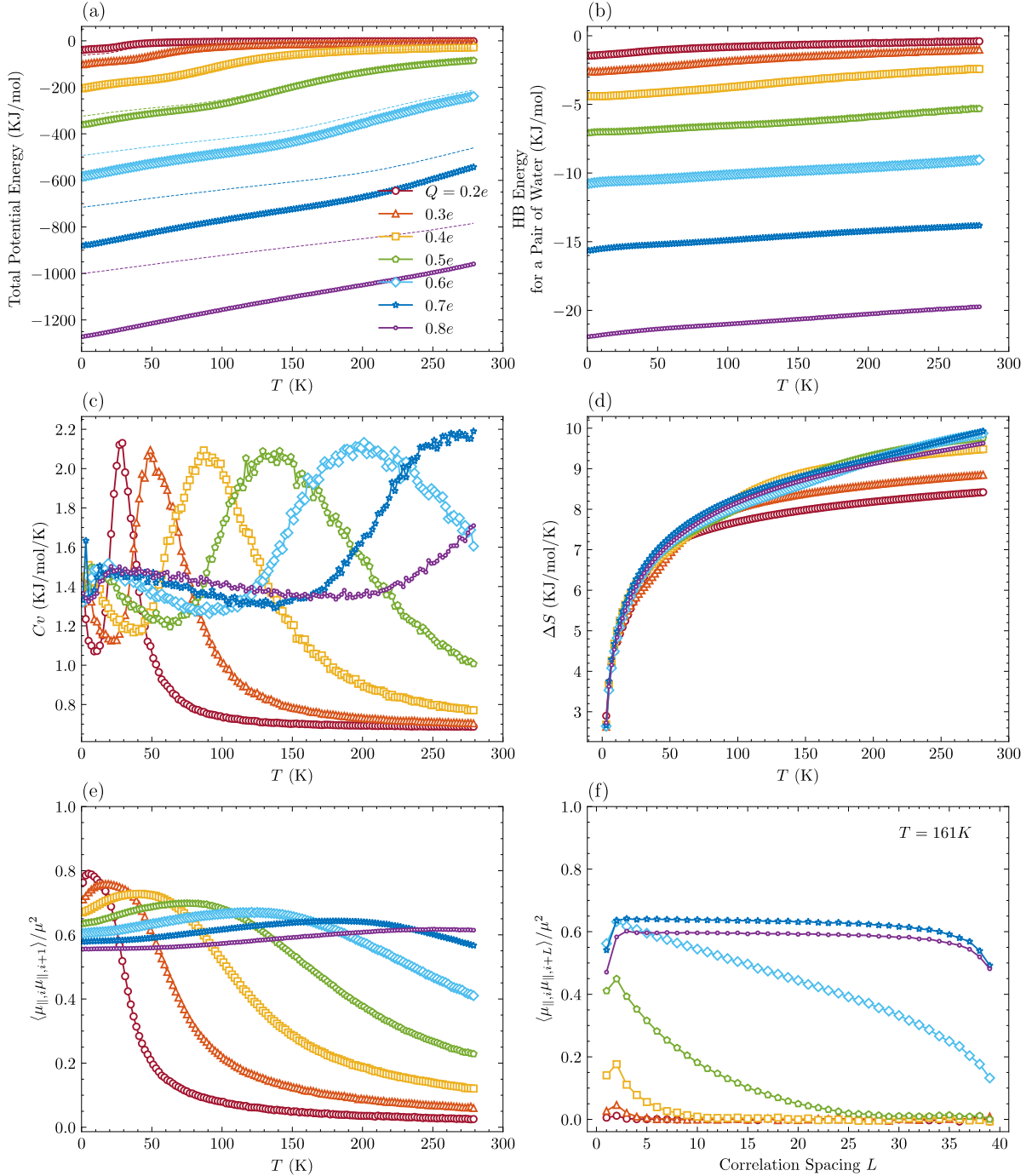


**FIG. 7.** Thermodynamic quantities of the single-file water chain with respect to temperature, for  $Q$  ranging from  $0.2e$  to  $0.8e$  with the increasement of  $0.1e$ , including (a) total potential energy (dashed lines) and electrostatic energy (dotted lines), (b) HB energy for a pair of water molecules, (c) heat capacity  $C_v$ , (d) entropy changes  $\Delta S$  with respect to  $T = 1$  K, (e) correlation of tangent component  $\mu_{||}$  and (f) dependence of correlation of  $\mu_{||}$  on two water molecules with the spacing  $L$  at a fixed temperature of  $161$  K.

The structural variations of the single-file water chain with respect to temperature at different values of  $Q$  suggests the significant influence of electrostatic interactions in quasiphase transitions. At a fixed temperature, the larger values of  $Q$  result in the lower total potential energy (dashed lines in Fig. 7(a)) and HB energy (Fig. 7(b)). For  $Q \geq 0.5e$ , the total potential energy is higher than the electrostatic energy within the whole temperature range, indicating that the electrostatic attraction dominates the interaction among water molecules such that the van der Waals interaction becomes repulsive. The increased electrostatic interaction pushes the quasiphases II, III and order-disorder transition to higher temperatures, as evidenced by the right shift of the minima in Fig. 7(d) from 10 K (0.2e) to 190 K (0.8e) and peaks from 30 K (0.2e) to 200 K (0.6e). The peaks for  $Q = 0.7e$  and  $0.8e$  are estimated to be above 279 K. In addition, the Schottky-like peak at lower temperatures, which is assumed to be induced by the excitation of rotational freedom from a completely HB bonded water chain, shifts from several Kelvin for smaller  $Q$  to about 30 K for  $Q = 0.8e$ . Despite the more ordered dipolar orientations in quasiphase II, the entropy of the single-file water chain in fact monotonically increases with respect to temperature for all  $Q$  values (Fig. 7(d)). The increased electrostatic attraction also moves the peak positions of correlation of tangent component  $\mu_{\parallel}$  of two neighbouring water molecules (Fig. 7(e), see PS. 4 in the Appendix for correlations of dipole vector  $\vec{\mu}_i$  and of normal component  $\mu_{\perp}$ ) to higher temperatures, and significantly extends the correlation from several water molecules to the whole water chain (Fig. 7(f), see PS.4 in the Appendix for other fixed temperatures).

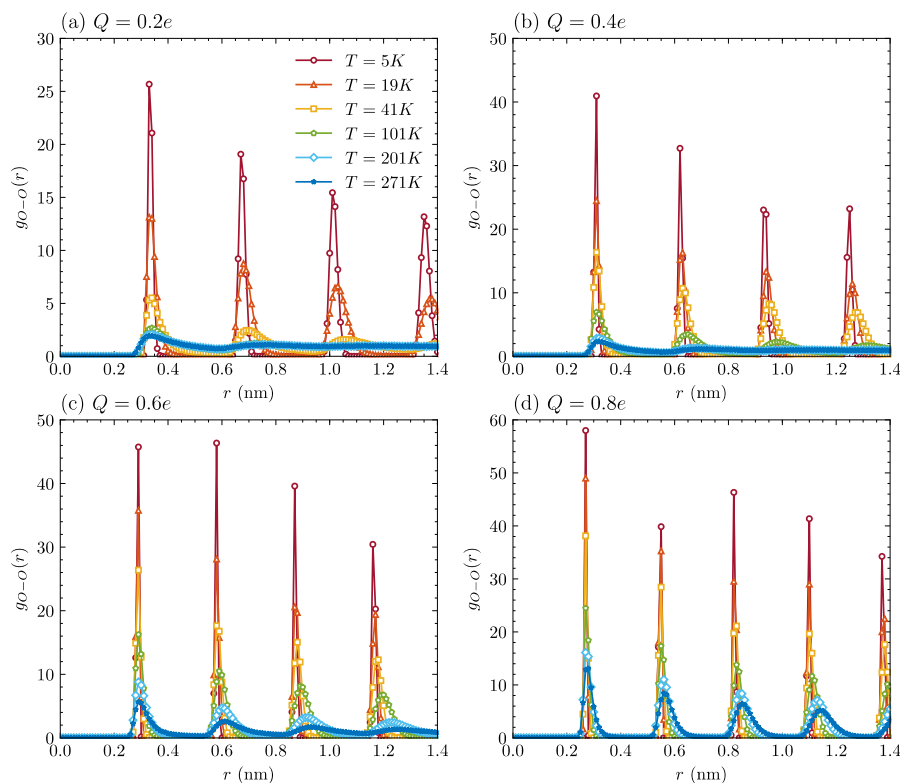
#### IV. CONCLUSIONS

In summary, we have performed orientational-biased replica exchange Monte Carlo simulations in the canonical ensemble to explore the quasiphase transition of a single-file water chain affected by the atomic charges in SPC/E water model. It has been demonstrated that the atomic charges play the critical role in the quasiphase transition of single-file water chain. Using the atomic charge as reported in literature, *i.e.*,  $q_O = -0.4328e$ , we have reproduced three distinct quasiphases comprising a fully hydrogen-bonded water chain at lower temperatures, a more ordered dipolar orientation along the  $x$ -axis at intermediate temperatures, and a completely disordered structure at higher temperatures. Then, we vary the atomic charge of  $q_O$  from  $-0.2e$  to  $-0.8e$  to explore how these values will affect the structural details and thermodynamic properties of quasiphase transitions. With the increase of magnitude of  $q_O$ , we find that the fragmentation of the entire water chain into shorter water segments, the orientational ordering of water dipoles, and the transition towards complete disorder are all inhibited. Consequently, the transition temperatures between three quasiphases have been shifted to higher temperatures. The thermodynamic analysis demonstrates that the larger atomic charge enhances the hydrogen bonding between neighbouring water molecules also the electrostatic attraction within the water chain, extending the spatial correlation of a pair of water dipoles. Our findings emphasize the importance of atomic charges of water models and electrostatic interaction in the study of water behavior under nanoconfinement.

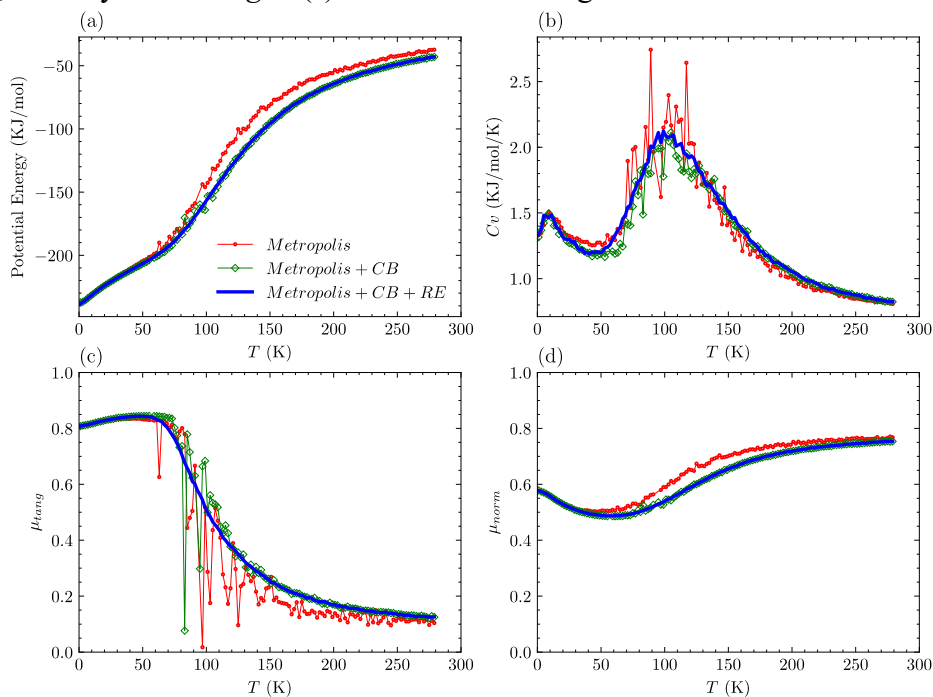
#### ACKNOWLEDGEMENT

We acknowledge the valuable discussion on the programming with Dr. Nan Sheng. This work was supported by the National Natural Science Foundation of China [Nos: 11605151, 12074394, 12075201]; the National Science Fund for Outstanding Young Scholars (No. 12022508). L. Zhao also acknowledge the computational resources provided by the Hefei

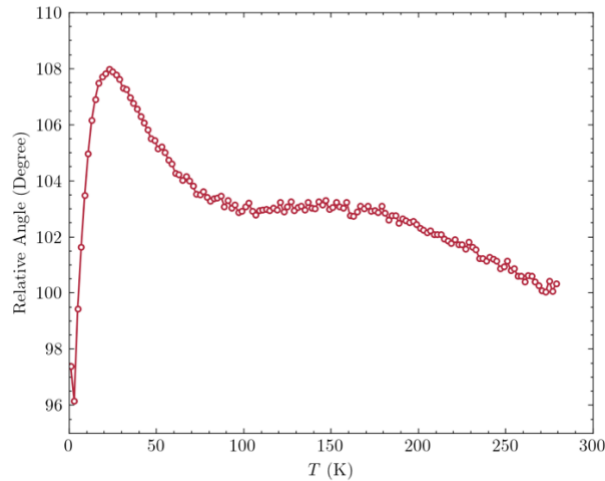
## APPENDIX



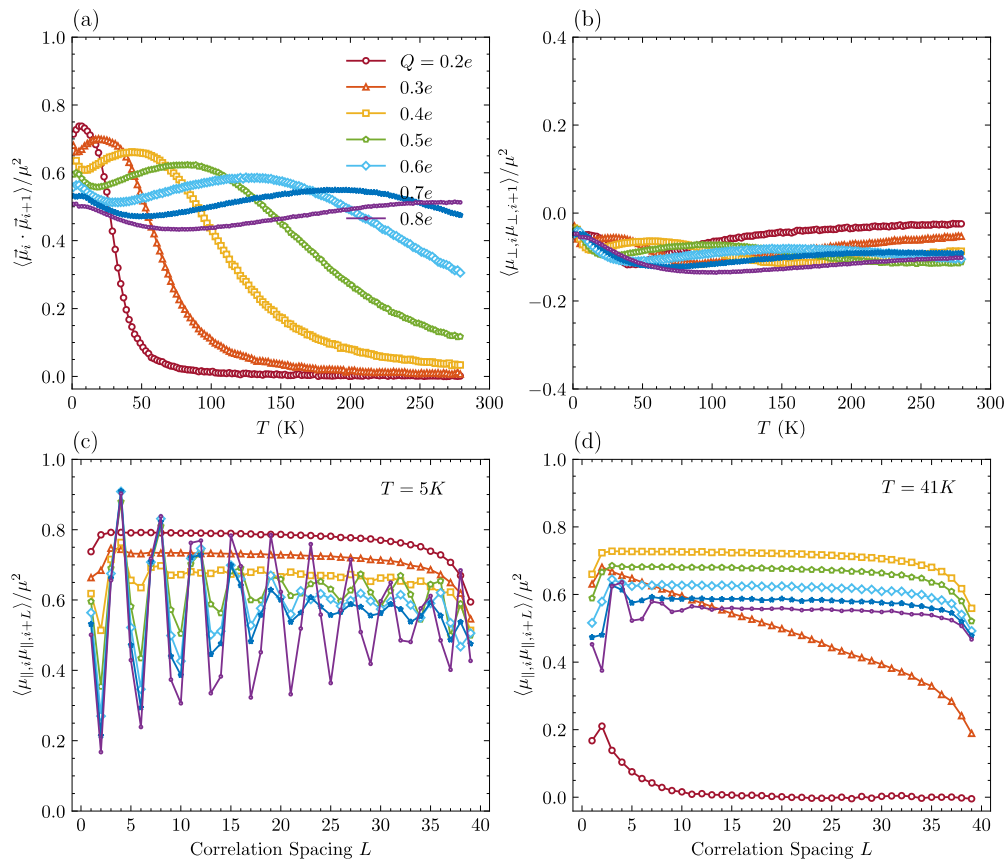
**PS. 1.** Radius distribution functions of two oxygen atoms,  $g_{O-O}(r)$ , at various temperatures under different  $Q$  values. The  $g_{O-O}(r)$  is defined by  $g_{O-O}(r) = \frac{1}{\bar{\rho}} \frac{\langle n(r) \rangle}{\Delta r}$ , where  $\langle n(r) \rangle$  is the ensemble average number of oxygen atoms in the interval  $[r, r + \Delta r]$  and  $\bar{\rho} = \frac{N}{L}$  is the average number density. The increment  $\Delta r$  is 0.01 nm. To identify the short-range arrangement of water molecules, we only show the  $g_{O-O}(r)$  in the distance range less than 1.4 nm.



**PS. 2.** Comparisons of analysis of (a) potential energy, (b) heat capacity  $C_v$ , (c)  $\mu_{tang}$  and (d)  $\mu_{norm}$  for  $Q = 0.4328e$  using three different Monte Carlo sampling methods including Metropolis-based translation/rotation algorithm (Metropolis), Metropolis translation/rotation plus the configuration bias methods (Metropolis + CB), and Metropolis translation/rotation plus the configuration bias and replica exchange methods (Metropolis + CB + RE). For Metropolis method, data are missing at  $T = 93$  K and  $95$  K due to that the average dipole angle of the single-file water chain  $\bar{\phi} > 90^\circ$ . Similar cases are at  $T = 57$  K and  $93$  K for Metropolis + CB method.



**PS. 3.** Relative angle of normal components  $\mu_{\perp}$  of two neighbouring water dipoles for  $Q = 0.4328e$  at different temperatures.



**PS. 4.** Correlations between neighbouring water molecules, including the correlations of (a) dipole vector  $\vec{\mu}_i$  and of (b) normal component  $\mu_{\perp}$ . (c) Dependence of correlation of  $\mu_{\parallel}$  on two water molecules with the spacing  $L$  at fixed temperatures of 5 K and 41 K.  $L$  represents the difference between indices of two molecules.

### References:

- [1] B. Lin, J. Jiang, X.C. Zeng, L. Li, Nat. Commun. **14**, 4110 (2023)
- [2] M.A. Belyanchikov, M. Savinov, Z.V. Bedran, P. Bednyakov, P. Proschek, J. Prokleska, V.A. Abalmasov, J. Petzelt, E.S. Zhukova, V.G. Thomas, A. Dudka, A. Zhugayevych, A.S. Prokhorov, V.B. Anzin, R.K. Kremer, J.K.H. Fischer, P. Lunkenheimer, A. Loidl, E. Uykur, M. Dressel, B. Gorshunov, Nat. Commun. **11**, 3927 (2020)
- [3] S. Chakraborty, H. Kumar, C. Dasgupta, P.K. Maiti, Acc. Chem. Res. **50**, 2139 (2017)
- [4] Q.L. Zhang, T. Zhou, C. Chang, S.Y. Gu, Y.J. Wang, Q. Liu, Z. Zhu, Phys. Rev. Lett. **132**, 184003 (2024)
- [5] J.C. Rasaiah, S. Garde, G. Hummer, Annu. Rev. Phys. Chem. **59**, 713 (2008)
- [6] A. Alexiadis, S. Kassinos, Chem. Rev. **108**, 5014 (2008)
- [7] A. Chatzichristos, J. Hassan, Nanomaterials (Basel) **12**, 174 (2022)
- [8] A. Barati Farimani, N.R. Aluru, J. Phys. Chem. B **115**, 12145 (2011)
- [9] X. Yang, F. Yu, L. Wang, R. Liu, Y. Xin, R. Li, Y. Shi, Z. Wang, J. Chem. Phys. **160**, 194904 (2024)
- [10] Z. Cao, Y. Peng, T. Yan, S. Li, A. Li, G.A. Voth, J. Am. Chem. Soc. **132**, 11395 (2010)
- [11] L. Wu, F. Wu, J. Kou, H. Lu, Y. Liu, Phys. Rev. E **83**, 061913 (2011)
- [12] Z. Wan, Y. Gao, X. Chen, X.C. Zeng, J.S. Francisco, C. Zhu, Proc. Natl. Acad. Sci. U.S.A. **119**, e2211348119 (2022)
- [13] K. Falk, F. Sedlmeier, L. Joly, R.R. Netz, L. Bocquet, Nano Lett. **10**, 4067 (2010)
- [14] J. Su, H. Guo, ACS Nano **5**, 351 (2011)
- [15] X. Zhou, F. Zhu, Phys. Rev. E **98**, 032410 (2018)
- [16] Y. Tu, P. Xiu, R. Wan, J. Hu, R. Zhou, H. Fang, Proc. Natl. Acad. Sci. U.S.A. **106**, 18120 (2009)
- [17] Z. Li, Q. Han, Y. Qiu, D. Wang, Carbon **202**, 83 (2023)
- [18] H. Fang, R. Wan, X. Gong, H. Lu, S. Li, J. Phys. D: Appl. Phys. **41**, 103002 (2008)
- [19] J. Kofinger, C. Dellago, New J. Phys. **12**, 093044 (2010)
- [20] J. Kofinger, G. Hummer, C. Dellago, J. Chem. Phys. **130**, 154110 (2009)
- [21] J. Kofinger, C. Dellago, Phys. Rev. Lett. **103**, 080601 (2009)
- [22] J. Kofinger, G. Hummer, C. Dellago, Proc. Natl. Acad. Sci. U.S.A. **105**, 13218 (2008)
- [23] T. Sahoo, D. Iouchtchenko, C.M. Herdman, P.N. Roy, J. Chem. Phys. **152**, 184113 (2020)
- [24] T. Serwatka, R.G. Melko, A. Burkov, P.N. Roy, Phys. Rev. Lett. **130**, 026201 (2023)
- [25] T. Serwatka, P.N. Roy, J. Chem. Phys. **156**, 044116 (2022)
- [26] R. Wan, J. Li, H. Lu, H. Fang, J. Am. Chem. Soc. **127**, 7166 (2005)
- [27] J. Li, X. Gong, H. Lu, D. Li, H. Fang, R. Zhou, Proc. Natl. Acad. Sci. U.S.A. **104**, 3687 (2007)
- [28] L. Jin, D. Zhang, Y. Zhu, X. Yang, Y. Gao, Z. Wang, J. Phys. Chem. Lett. **12**, 350 (2021)
- [29] J. Chen, X.Z. Li, Q. Zhang, A. Michaelides, E. Wang, Phys. Chem. Chem. Phys. **15**, 6344 (2013)
- [30] X. Ma, S. Cambre, W. Wenseleers, S.K. Doorn, H. Htoon, Phys. Rev. Lett. **118**, 027402 (2017)
- [31] M. Druchok, V. Krasnov, T. Krokhmalkii, E.B.T. Cardoso, S. Martins de Souza, O. Rojas, O. Derzhko, J. Chem. Phys. **158**, 104304 (2023)
- [32] M. Druchok, V. Krasnov, T. Krokhmalkii, O. Derzhko, J. Mol. Liq. **387**, 122633 (2023)
- [33] L. Wang, J. Zhao, F. Li, H. Fang, J.P. Lu, J. Phys. Chem. C **113**, 5368 (2009)
- [34] D. Frenkel, B. Smit, Understanding molecular simulation: from algorithms to applications, Elsevier2023.
- [35] D. Landau and K. Binder, A Guide to Monte Carlo Simulations in Statistical Physics, Second Edition,

Cambridge University Press

[36] L. Zhao, S. Xu, Y. Tu, X. Zhou, *Chin. Phys. B* **26**, 060202 (2017)

[37] G.N. Sarkisov, V.G. Dashevsky, G.G. Malenkov, *Mol. Phys.* **27**, 1249 (1974)